Research and Reviews in Materials Science and Chemistry
Vol. 8, Issue 1, 2018, Pages 21-57
ISSN 2319-6920
Published Online on June 16, 2018
© 2018 Jyoti Academic Press
http://jyotiacademicpress.org

PREPARATION AND CHARACTERIZATION OF MANGANESE OXIDE BASED GRAPHITE USING WET ATTRITION TECHNIQUE AND ITS APPLICATION IN REMOVAL OF METHYLENE BLUE DYE FROM AQUEOUS SOLUTION

A. I. ABD EL-HAMID and HESHAM M. A. SOLIMAN

Composites and Nanostructured Materials Research Department
Advanced Technology and New Materials Research Institute
City of Scientific Research and Technological Applications (SRTA-City)
New Borg El-Arab
21934 Alexandria
Egypt
e-mail: ahm_ch_ibr@yahoo.com

Abstract

This work reports approach of facile and one-step synthesis of manganese oxidegraphite (MnO_x-G) composite and its catalytic activity towards degradation of methylene blue (MB) dye. The composite was characterized by using SEM/EDS, XRD, and FTIR. Degradation reaction of MB was investigated by varying composite doses, MB concentrations, temperatures and pH values. The residual concentration of the dye in the aqueous solution was determined using UV-Vis spectrophotometer. The kinetics of adsorption step was described by pseudo first-order and pseudo-second order kinetic models. The pseudo-second order well fitted the experimental data. Moreover, Langmuir-Hinshelwood (L-H) model pseudo first order was utilized to evaluate the degradation reaction rate at different experimental conditions. Degradation

Keywords and phrases: methylene blue, degradation, adsorption, manganese oxide, graphite.
Communicated by Dorina Simedru.
Received March 7, 2018; Revised April 4, 2018; Re-Revised May 11, 2018

reaction rate has increased with the increase in composite dose to a certain point after which the rate decreased. Also, the degradation rate increased proportionally with temperature, while inversely proportional with dye concentration and pH value. A simple mechanism for adsorption and degradation of the dye over the composite was proposed.

1. Introduction

Nowadays, the industrial wastewater considers a one from essential sources that introducing the pollutants in the environment. However, effluents from textile and dyeing industries containing synthetic dyes and pigments are considered as environmental hazardous that cause messing up of drinking water and sometimes characterized as a carcinogenic [1]. The presence of the dye in water even at very low concentrations was harmful to the underwater plants [2], where the dyes interfere with water properties and inhibit the penetration of sun light causing reduction of the photosynthesis process.

Methylene blue (MB) dye is used in various applications such as dyeing cotton, wood, silk, furthermore, MB is commonly used as a photodynamic anti-microbial agent in biological materials, moreover, MB act as a photosensitizer in solar cells and a surface modifier of semiconductor colloids and a test compound in semiconductor photocatalysis [3]. However, MB-dye has a harmful effects on both human and animals that causes permanent burn in eyes nausea, vomiting, and methemoglobinemia [4]. Therefore, it is necessary to remove MB industrial wastewater before it damages the natural environment.

Manganese oxides are natural occurring materials that are widely extended in soils and sediments. Because of their excellent semiconductivity, porosity, and mixed-valent property, manganese oxides have also been used or synthesized recently as a catalyst via the re-oxidation of manganese from a lower valence to a higher valence in many technological applications [3]. With reducing potential between 1.27V-1.5V [5], MnO_x acts as potential oxidant and diminished the toxicity of organic and inorganic materials [6, 7].

Manganese oxide is required in a wide applications in water treatment [8, 9], this is attributed to its ability to form multi-oxidation states (MnO, MnO_2, Mn_2O_3, and Mn_3O_5) [10].

MnO_x particles in the nanoscale tend to aggregate as well as become less stable, which leads to decrease their catalytic efficiency, moreover, the difficulty of removing these nanomaterials from the treated water, it becomes more interest to support MnO_x nanoparticles on a suitable substrate to give a good separately and remarkable oxidation properties for the treated wastewater.

In this study, MnO_x nanoparticles supported by graphite flakes were prepared using wet attrition process as a green, simple and low cost technique. The composite prepared was used to remove MB dye from water. The effect of sample dosage, dye concentration, initial pH, and temperature on the removal rate of the dye was investigated.

2. Experimental

2.1. Materials and instrumentation

All chemicals were of analytical grade and used as received. Methylene blue (MB) was purchased from Sigma-Aldrich. Water distillatory (2108, GLF, Germany), pH meter (3510, Genway), Hot plate stirrer (SB 162, Stuart, UK), Centrifuge, (Mikro 220R, Hettich, UK), UV/Vis. Spectrophotometer-Double beam (T80+, PG instruments Ltd., UK), Analytical balance (CP 2245, Sartorius, USA) and ball mill (Retsch-PM400) were used during the experimental preparations and investigation.

Surface morphologies of nanoparticles were investigated by using scanning electron microscopy (SEM) “Jeol Japan –JSM-636 OLA”, while elemental analysis was achieved using SEM-EDS unit. Crystallinity of particles was determined by X-ray diffraction (XRD) “Shimadzu, Japan XRD – 7000”. Various vibration modes were performed by Fourier transmission infrared spectroscopy (FTIR) “Shimadzu, Japan-8400s”.

2.2. Preparation of manganese oxide-graphite (MnO_x-G) composite

MnO_x-G composite was prepared using wet attrition technique. Briefly, 5g of graphite, 6g of potassium permanganate, and 4g of sodium nitrite were charged in a laboratory scaled ball mill. Steel balls were used as milling media, 250ml steel vial was used as a reactor and the ball mill was adjusted at 400rpm on a "continuous mode". A milling period of 8 hr, media weight of 113g and ethanol volume of 50ml were taken as milling conditions. The produced composite was then separated by filtration, washed several time with distilled water and finally washed by 200ml hot distilled water, then dried at 110°C for 24 hr.

2.4. Catalytic degradation and removal efficiency

The dye degradation by MnO_x-G was studied by monitoring the color change of the MB dye in an aqueous solution under continuous stirring. The experiments were carried out in a glass beaker where different amounts of composite (10mg, 25mg, 50mg, and 100mg) were added into four beakers each of them containing 10ml aqueous solution of certain concentration of MB dye. The dye concentration was 100ppm, 150ppm, 200ppm, and 300ppm, temperature (25°C, 40°C, 60°C, and 80°C) and pH (1.5, 3, 7, 9, and 11). 0.5ml of the suspension was removed and centrifuged. After phase separation 0.1ml of the centrifuged solution was diluted to 10ml by distilled water and MB concentration was determined at 662nm, 293nm, and 243nm.

The dye removal efficiency (Deg.%) is defined as:

$$\text{Deg.\%} = \frac{(C_0 - C_t)}{C_0} \times 100, \tag{1}$$

where, C_0 and C_t are the initial concentration and the concentration of dye at time *t*, respectively.

2.5. Kinetic study

2.5.1. Adsorption kinetic

2.5.1.1. Pseudo first order kinetic model

The adsorption kinetics can be described by a pseudo-first order equation as suggested by Lagergren [11]:

$$\log(q_e - q_t) = \log q_e + \frac{K_{ad}t}{2.303}, \tag{2}$$

where q_e(mg/g) is the amount of sorption at equilibrium time, q_t(mg/g) is amount of sorption at time t, $K_{ad}(\min^{-1})$ is the rate constant of pseudo first order sorption. Values of K_{ad} were calculated from the slope of linear plots of log $(q_e - q_t)$ versus t.

$$q_e = \frac{(C_0 - C_e)V}{1000w}, \tag{3}$$

where C_0 is the initial concentration (mg/L), C_e is the dye concentration at equal time intervals (mg/L), V is the volume of dye solution (mL), w is the mass of adsorbent (g).

$$q_t = \frac{(C_0 - C_t)V}{1000w}, \tag{4}$$

where C_t is the dye concentration at different time intervals (mg/L).

2.5.1.2. Pseudo second order kinetic model

The pseudo second order equation developed by Ho and McKay [12] has a linear form as:

$$\frac{t}{q_t} = \frac{1}{K_2 q_e^2} + \frac{t}{q_e}, \tag{5}$$

where $K_2(\text{g mg}^{-1}\ \text{min}^{-1})$ is the rate constant of pseudo second order reaction.

2.5.2. Catalytic kinetic (first order kinetic model)

$$\ln \frac{A_o}{A} = Kt, \tag{6}$$

where A_o the absorbance of MB at $t = 0$, A the absorbance of MB at different time intervals, and $K(\min^{-1})$ is the apparent rate constant.

3. Results and Discussion

3.1. Characterization

The morphology of the precursor graphite (pr-G) and MnO_x-G composite at different magnifications was investigated by SEM, as shown in Figure 1. The pr-G seems as compacted flakes-like structure, as in Figure 1(a)-(c) (left). The SEM micrographs of MnO_x-G composite indicate that the MnO_x nanoparticles were emerged everywhere on the surface and within the graphite flakes, as demonstrated in Figure 1(d)-(f) (right). Consequently, MnO_x will be highly dispersed on the graphite layer and accordingly the catalytic activity should enhance dramatically.

[I] Precurosor graphite

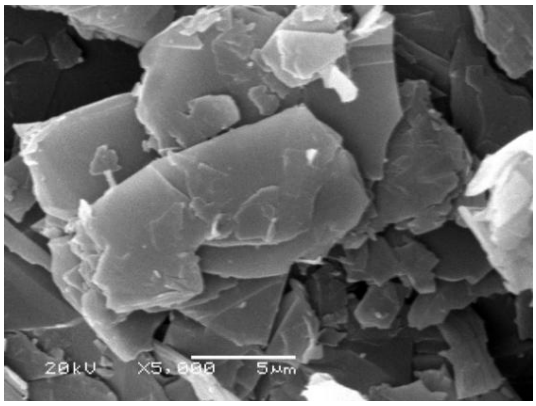

(a)

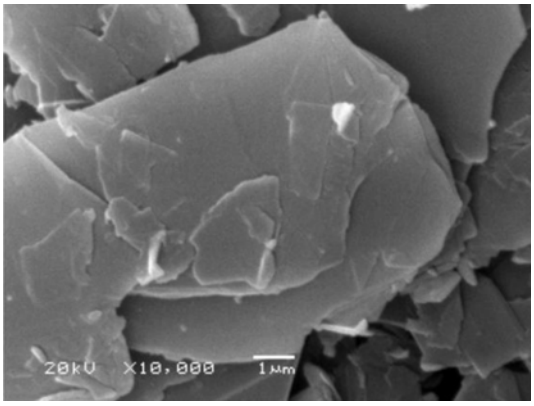

(b)

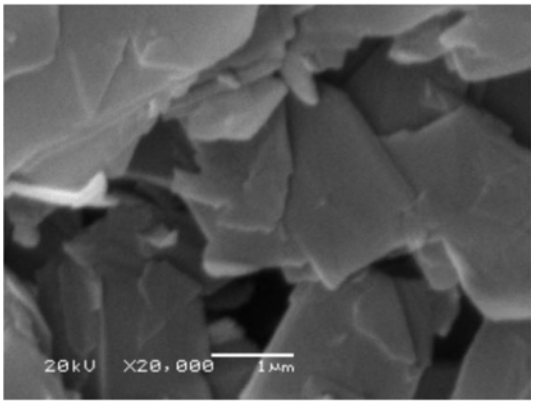

(c)

[II] MnO_x-graphite composite

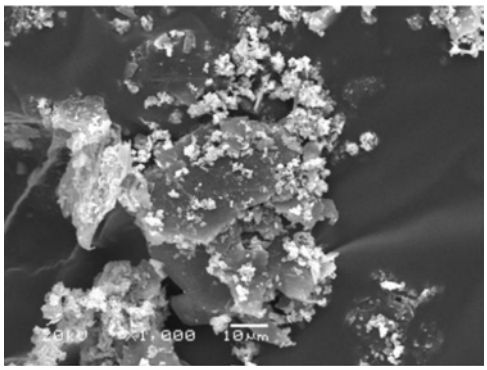

(d)

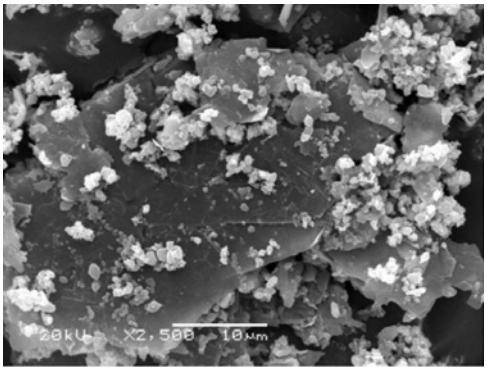

(e)

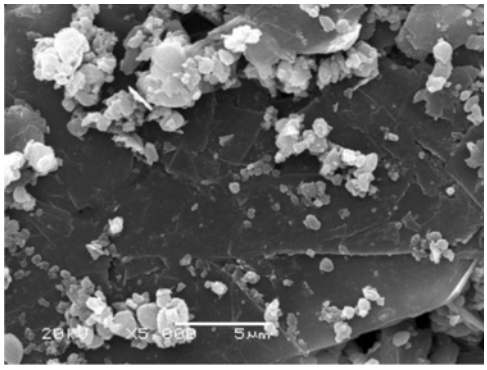

(f)

Figure 1. SEM image of [I] precursor graphite ((a), (b) and (c)) and [II] the MnO_x-graphite (MnO_x-G) composite ((d), (e) and (f)).

The XRD patterns of pr-G, MnO_x, and (MnO_x-G) composite are presented in Figure 2. It is clear that from Figure 2(a), the Pr-G shows a sharp diffraction peak at 26.8°, this peak characterized the crystalline structure of the graphite. The diffractogram reveals that MnO_x does not show any narrow peak, which proves the amorphous structure of emerged nanoparticles as in Figure 2(b). MnO_x-G composite shows XRD patterns (Figure 2(c)) which combine of the XRD patterns of both pr-G and MnO_x.

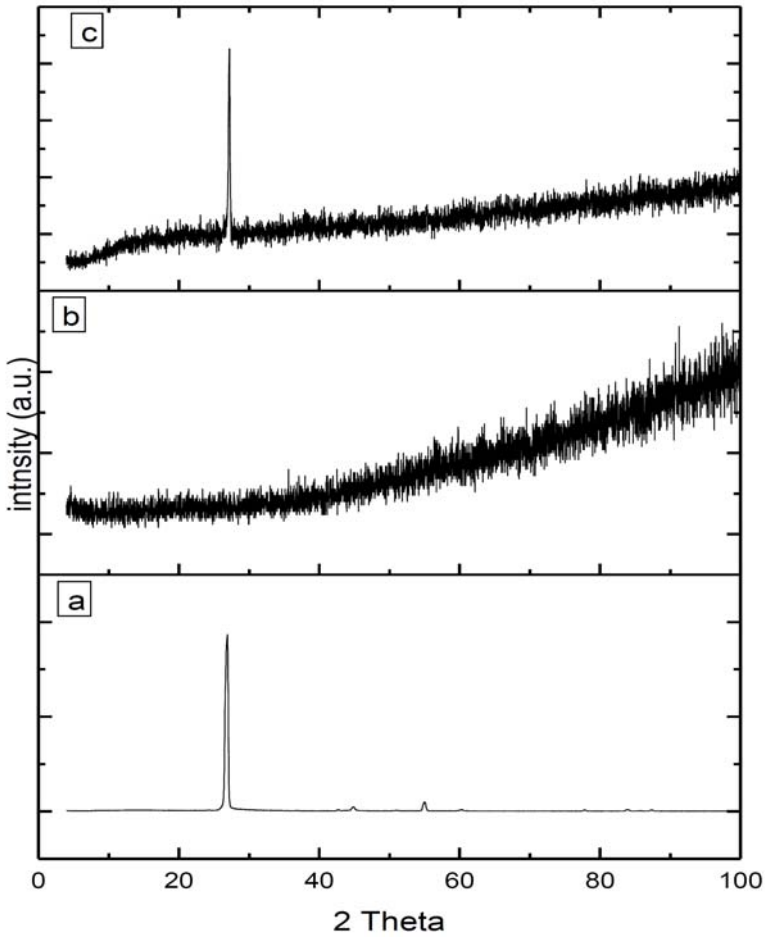

Figure 2. XRD patterns of (a) pr-G, (b) MnO_x, and (c) MnO_x-G composite.

The basic chemical compositions of pr-G and (MnO_x-G) composite were determined by EDS analysis as demonstrated in Figure 3. The EDS spectrum, Figure 3(a), showed that the pr-G mainly composed of carbon (At% = 100). On the other hand, the elemental composition of (MnO_x-G) composite (Figure 3(b)) showed that the composition of the composite is C (At% = 41.01), O (At% = 31.72), Mn (At% = 15.97), Na (At% = 7.61), and K (At% = 3.68). The atomic ratio of Mn:O is 1:2 and the traces of Na and K came from $NaNO_2$ and $KMnO_4$, respectively.

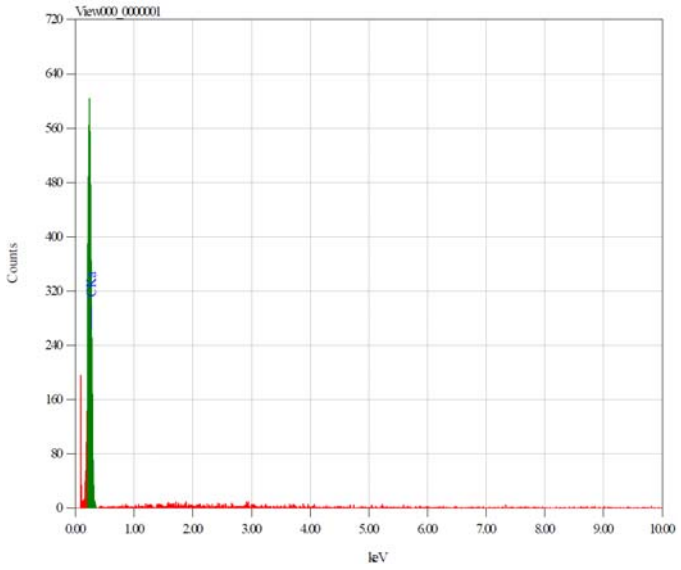

(a)

Element	(keV)	mass%	Error%	At%	K
C K	0.277	100.00	2.72	100.00	100.0000
Total		100.00		100.00	

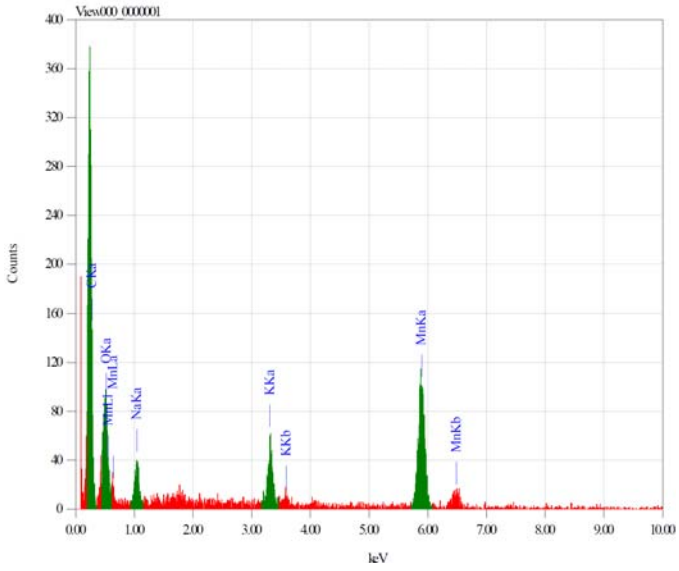

(b)

Element	(keV)	mass%	Error%	At%	K
C K	0.277	22.43	0.93	41.01	9.4826
O K	0.525	23.10	1.63	31.72	23.6637
Na K	1.041	7.97	1.75	7.61	5.1872
K K	3.312	6.55	1.00	3.68	10.0051
Mn K	5.894	39.95	2.57	15.97	51.6614
Total		100.00		100.00	

Figure 3. EDS analysis of (a) graphite and (b) MnO_x-graphite (MnO_x-G) composite.

FTIR was used to detect the functional groups within the material under investigation. Figure 4, summarizes the FTIR of pr-G, MnO_x-G composite, MB dye, and MnO_x-G-MB complex composite after interaction with the dye solution. According to the FTIR spectrum of pr-G (Figure 4(a)) there is a broad wide band at ~ 3433cm^{-1} reveals to the O-H stretching of hydroxyl group, Figure 4(b), which refers to (MnO_x-G) composite, shows two broad bands at ~ 3433cm^{-1} and ~ 530cm^{-1}

corresponding to OH stretching and Mn-O stretching vibration [13]. The FTIR bands which reveals to MB dye are shown in Figure 4(c). After the water treatment process, MnO_x-G composite shows FTIR spectrum (Figure 4(d)) with absence of the MB-dye peaks, this affirms the catalytic degradation approach of MnO_x-G composite.

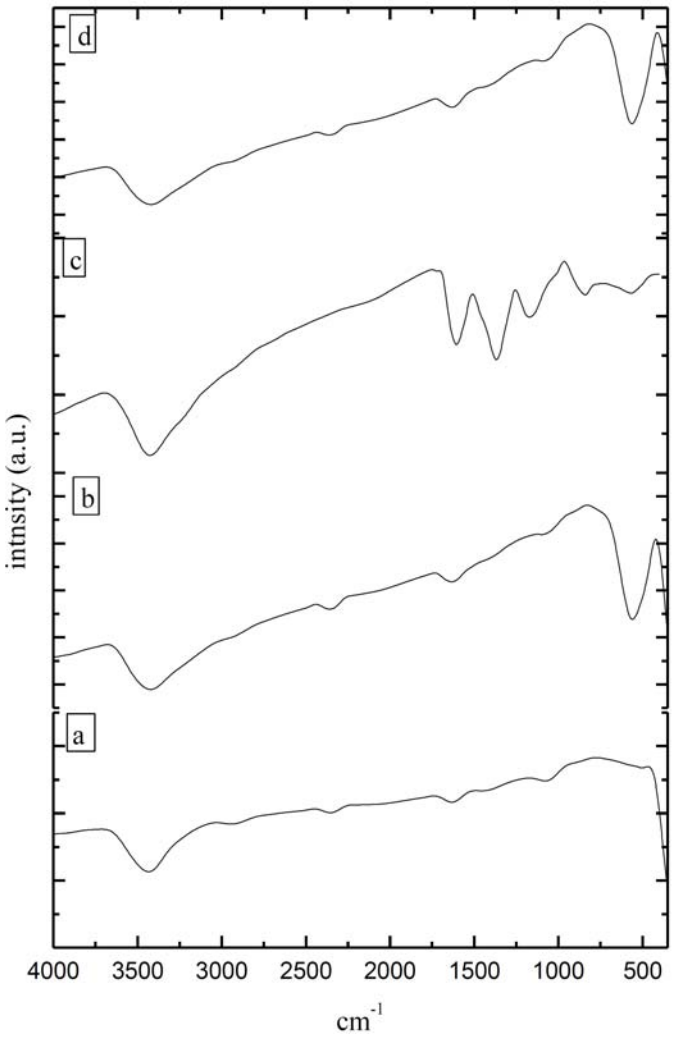

Figure 4. FTIR spectrum of (a) pr-G, (b) MnO_x-G composite, (c) MB dye, and (d) MnO_x-G composite after interaction with the dye solution.

3.2. Influence of experimental parameters

3.2.1. Composite dose

Experiments performed with different doses of the catalyst (Figure 5(a)), show that the removal percent (%R) increases with increasing the catalyst amount to certain extent after which the %R start to decrease. This is attributed to increasing the number of available active sites with increasing of the amount catalyst dose, as a result, the removal percent increase. Moreover, at addition of the solid to the dye solution with high dose, the solid composite tend to agglomerate, resulting in reduction of number of available active sites and decreases the removal percent [14, 15].

The information calculated from the pseudo first-order and pseudo second-order kinetic models plots (Figure 5(b) and (c), respectively) at different MnO_x-G dose are presented in Table 1. It is indicated that the pseudo second-order kinetic model has a high correlation coefficient $(R^2 > 0.97)$, moreover, the values of adsorption equilibrium (q_e) calculated much closer to the q_e calculated form the experiment than that calculated from the pseudo first-order. Therefore, it can be concluded that the pseudo second-order kinetic model is the best fit for the experimental data.

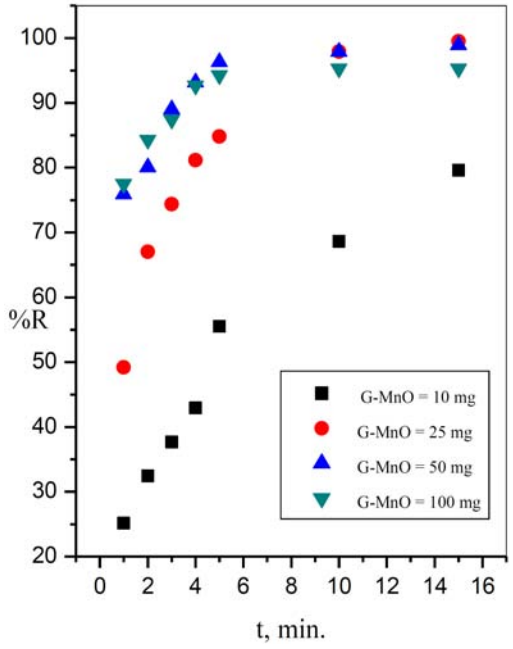
%R
t, min.
G-MnO = 10 mg
G-MnO = 25 mg
G-MnO = 50 mg
G-MnO = 100 mg

(a)

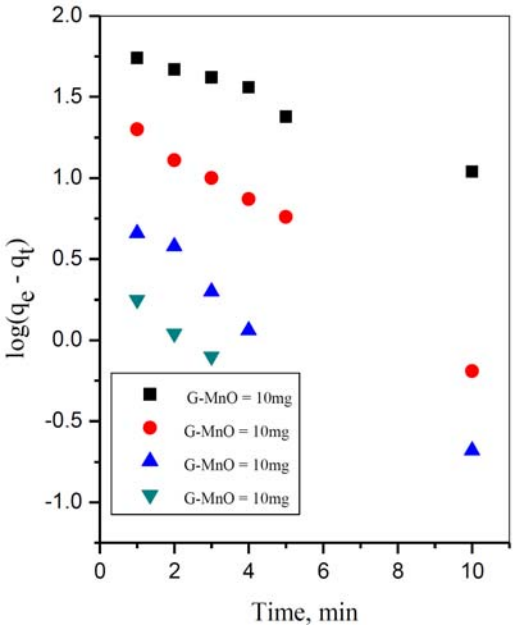
log(qe - qt)
Time, min
G-MnO = 10mg
G-MnO = 10mg
G-MnO = 10mg
G-MnO = 10mg

(b)

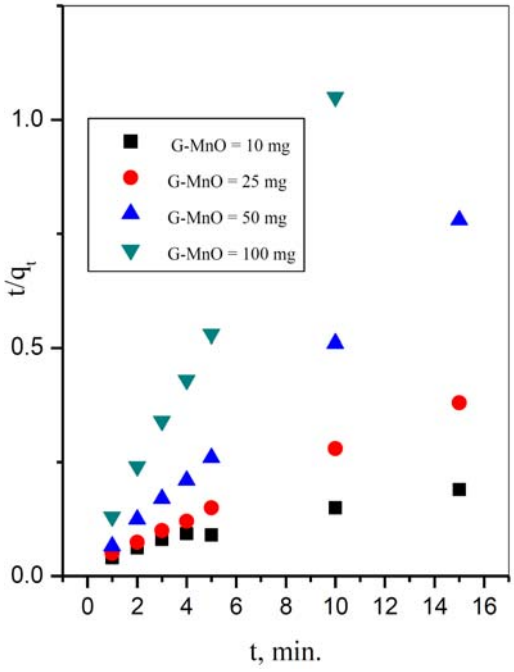
G-MnO = 10 mg
G-MnO = 25 mg
G-MnO = 50 mg
G-MnO = 100 mg
t/q_t
t, min.

(c)

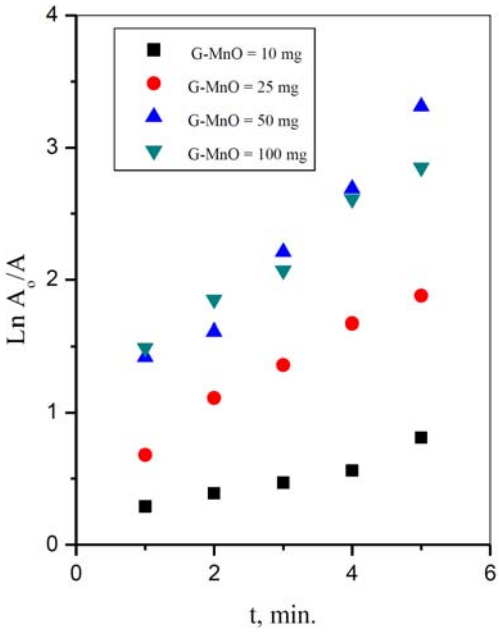
G-MnO = 10 mg
G-MnO = 25 mg
G-MnO = 50 mg
G-MnO = 100 mg
Ln A_o/A
t, min.

(d)

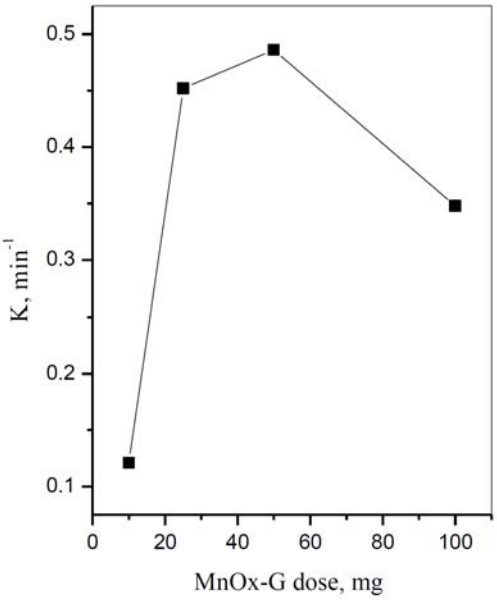

(e)

Figure 5. Effect of composite dose on (a) removal percent (%R) of the dye, (b) pseudo first-order kinetic model, (c) pseudo second-order kinetic model, (d) ln (A_o/A) for the catalytic degradation, and (e) change in reaction rate with catalyst dose. ([MB] = 100ppm, pH = 7 and T = 25°C).

Table 1. Calculated parameters of the pseudo first-order and pseudo second-order kinetic models for various MnO_x-G doses

Adsorbent dose, mg	$q_{e\,\exp}$(mg/g)	First-order kinetic parameter		
		$K_1(\min^{-1})$	$q_{e\,\mathrm{cal}}$(mg/g)	R^2
0.01	79.60	– 0.18	67.61	0.981
0.025	39.80	– 0.83	30.90	0.899
0.05	19.80	– 0.83	5.70	0.940
0.10	9.53	– 0.71	4.41	0.977

Adsorbent dose, mg	$q_{e\,\exp}$(mg/g)	Second-order kinetic parameter		
		K_2(g mg^{-1} min^{-1})	$q_{e\,\mathrm{cal}}$(mg/g)	R^2
0.01	79.60	3.62×10^{-3}	87.60	0.970
0.025	39.80	0.02	41.67	0.972
0.05	19.80	0.17	20.00	0.997
0.10	9.53	0.39	9.80	0.999

The catalytic degradation kinetic of some organic dye species use Langmuir-Hinshelwood (L-H) model pseudo first order to evaluate the degradation reaction rate [15]. The model determines the relation between the initial degradation rate and initial concentration of organic adsorbate. L-H model can be expressed by Equation (6).

The inset of Figure 5(d) shows a good linear relationship between ln (A_o/A) versus reaction time for various catalyst dose and the rate constant (k) was calculated from the obtained slopes. Figure 5(e) presents the relation between K and the catalyst dose amount. The figure shows that at the beginning, the rate increases with increase of the catalyst amount. However, at higher amount of composite dose (> 50mg) the degradation rate decreases. This is referring to the rate of degradation reaction highly affected by the adsorption process [16, 17], where, the dye species transfer from the bulk of solution to the surface of catalyst by adsorption process.

3.2.2. Dye concentration

The degradation of MB was carried out over a constant condition of T = 25.0°C, pH = 7.0 and catalyst concentration = 25mg/10ml within 15 min for various dye concentrations. As indicated from Figure 6(a), the removal percent of the dye decreases with increasing the dye concentration in the range (100, 150, 200, and 300mg/L). This is due to, increase the number of the dye species in the aqueous solution, as a result of increasing in the concentration of the dye, while, the number of available active sites are limited, this leads to decrease the degradation percent [18]. Moreover, the increase in the number of substrate ions accommodating in the interlayer spacing inhibits the action of catalyst [19].

The adsorptions kinetic models; pseudo first order and pseudo second order were plotted at various concentration of MB dye as presented in Figure 6(b) and (c), respectively. The kinetic parameters were calculated and the correlation coefficients obtained are listed in Table 2. From the R^2 values (> 0.990) and the calculated q_e values, it can be demonstrated that the pseudo second order adsorption kinetic models fitted well the experimental data.

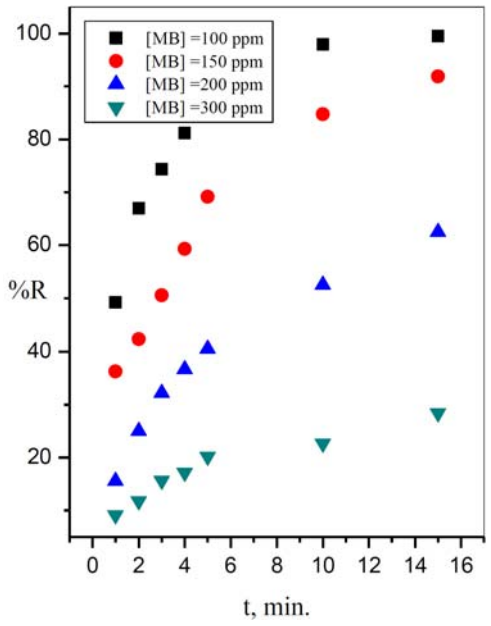
[MB] =100 ppm
[MB] =150 ppm
[MB] =200 ppm
[MB] =300 ppm
%R
t, min.

(a)

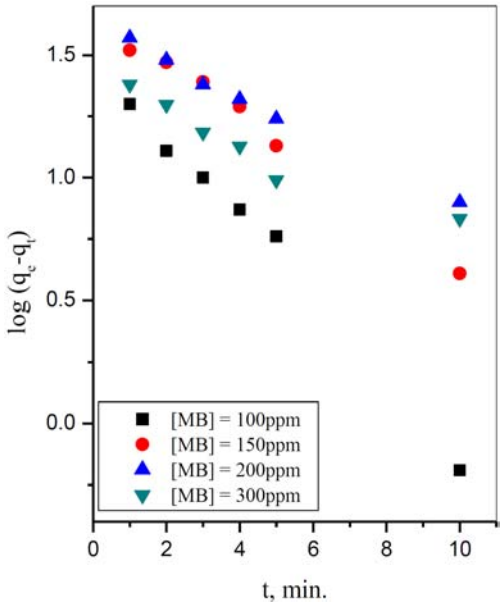
log (qe-qt)
[MB] = 100ppm
[MB] = 150ppm
[MB] = 200ppm
[MB] = 300ppm
t, min.

(b)

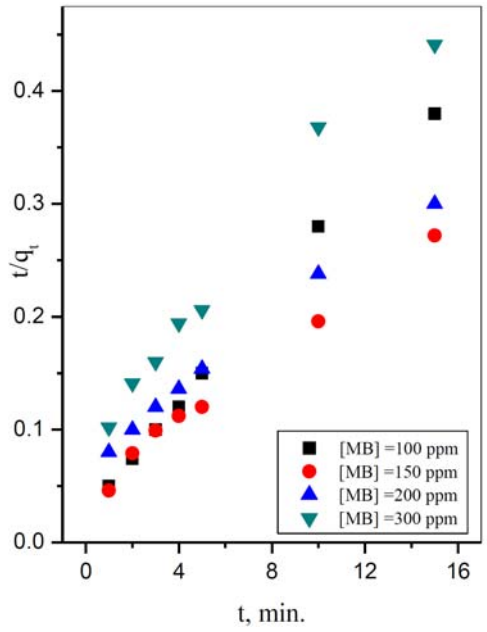
0.4
0.3
0.2
0.1
0.0
t/q_t
0
4
8
12
16
t, min.
[MB] =100 ppm
[MB] =150 ppm
[MB] =200 ppm
[MB] =300 ppm

(c)

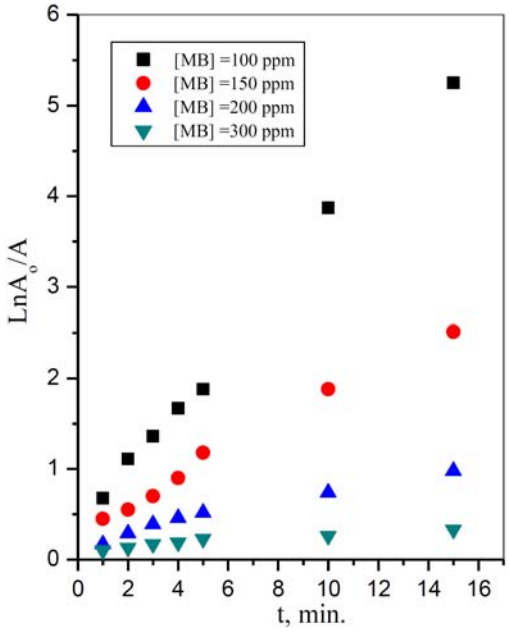
6
5
4
3
2
1
0
LnA_o/A
0
2
4
6
8
10
12
14
16
t, min.
[MB] =100 ppm
[MB] =150 ppm
[MB] =200 ppm
[MB] =300 ppm

(d)

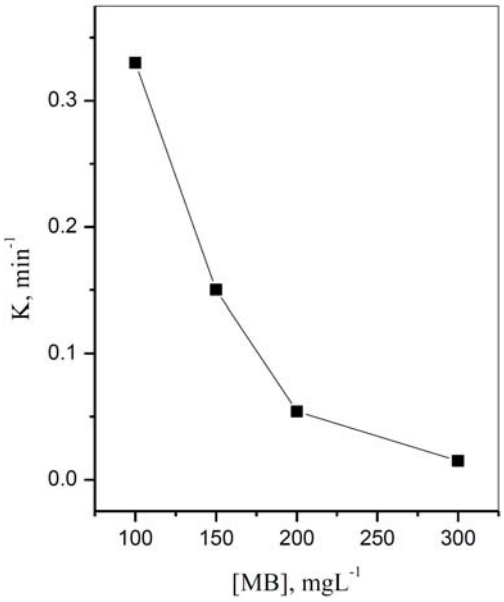

(e)

Figure 6. Effect of MB dye concentration on (a) removal percent (%R) of the dye, (b) pseudo first-order kinetic model, (c) pseudo second-order kinetic model, (d) ln (A_o/A) for the catalytic degradation, and (e) change in reaction rate with dye concentration. (Catalyst concentration = 25mg/10ml, pH = 7 and T = 25ºC).

Table 2. Calculated parameters of the pseudo first-order and pseudo second-order kinetic models for various concentration of MB

[MB], ppm	$q_{e\,\exp}$(mg/g)	First-order kinetic parameter		
		$K_1(\min^{-1})$	$q_{e\,\mathrm{cal}}$(mg/g)	R^2
100	37.80	– 0.38	30.90	0.899
150	55.12	– 0.24	46.77	0.987
200	50.00	– 0.17	41.70	0.988
300	34.00	– 0.14	24.55	0.993

[MB], ppm	$q_{e\,\exp}$(mg/g)	Second-order kinetic parameter		
		K_2(g mg^{-1} min^{-1})	$q_{e\,\mathrm{cal}}$(mg/g)	R^2
100	37.80	0.02	41.67	0.997
150	55.12	5.70×10^{-3}	62.50	0.990
200	50.00	4.60×10^{-3}	57.50	0.993
300	34.00	0.011	34.50	0.992

Different dye concentrations gave linear correlations between ln (A_o/A) and the reaction time (Figure 6(d)) indicating the degradation reaction is a pseudo first order kinetic reaction. The rate constants were calculated from the obtained slopes. By plotting the rate constants vs. different dye concentrations (Figure 6(e)), it is clear that the kinetic rate constant decreases with the increase in dye concentration.

3.2.3. Temperature

The catalytic degradation studies were carried out at 25ºC, 45ºC, 60ºC, and 80ºC and the results of these experiments are shown in Figure 7(a). It is clear from the figure that the used temperature range has not influenced on removal of MB-dye, where the removal percent at 25ºC (91.86), 45ºC (92.88), 60ºC (94.24), and 80ºC (92.54).

The linear relation of pseudo first order and pseudo second order adsorption kinetic models are shown in Figure 7(b) and (c). The calculated values of q_e and correlation coefficients R^2 are summarized in Table 3. The values of R^2 obtained from pseudo first order model was ≤ 0.990, while in case of pseudo second order adsorption model R^2 ≥ 0.990. Moreover, the calculated values of q_e agree very well with the experimental data. This indicates that the reactions kinetic of the adsorption process is more likely flow the pseudo second order models.

Table 3. Calculated parameters of the pseudo first-order and pseudo second-order kinetic models at different temperatures

T, °C	$q_{e\,\exp}$(mg/g)	First-order kinetic parameter		
		$K_1(\min^{-1})$	$q_{e\,\mathrm{cal}}$(mg/g)	R^2
25	55.12	0.24	46.77	0.988
45	55.73	0.38	41.90	0.990
60	56.54	0.49	33.90	0.979
80	55.52	0.39	19.10	0.860

T, °C	$q_{e\,\exp}$(mg/g)	Second-order kinetic parameter		
		K_2(g mg^{-1} min^{-1})	$q_{e\,\mathrm{cal}}$(mg/g)	R^2
25	55.12	5.70×10^{-3}	62.57	0.990
45	55.73	0.013	62.50	0.999
60	56.54	0.046	55.56	0.998
80	55.52	0.032	58.82	0.999

The apparent pseudo first order constants at different temperatures were evaluated by plotting the natural logarithm of A_o/A as a function of time using the first order kinetic analysis as shown in Figure 7(d). The relation between the rate constant and temperature was investigated as presented in Figure 7(e). From the graph, it can be concluded that by increasing the temperature the degradation rate increases.

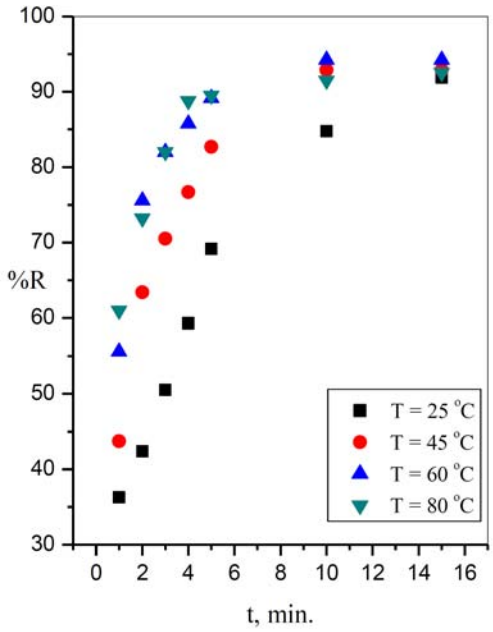
100
90
80
70
%R
60
50
40
30
0
2
4
6
8
10
12
14
16
t, min.
T = 25 °C
T = 45 °C
T = 60 °C
T = 80 °C

(a)

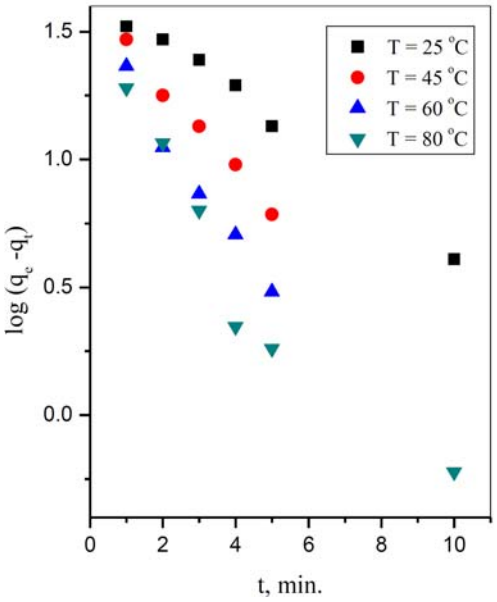
1.5
1.0
0.5
0.0
log (qe -qt)
0
2
4
6
8
10
t, min.
T = 25 °C
T = 45 °C
T = 60 °C
T = 80 °C

(b)

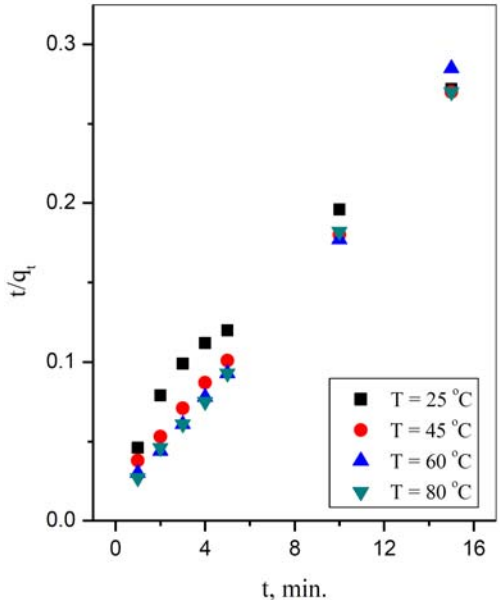
0.3
0.2
0.1
0.0
t/q_t
0
4
8
12
16
t, min.
T = 25 °C
T = 45 °C
T = 60 °C
T = 80 °C

(c)

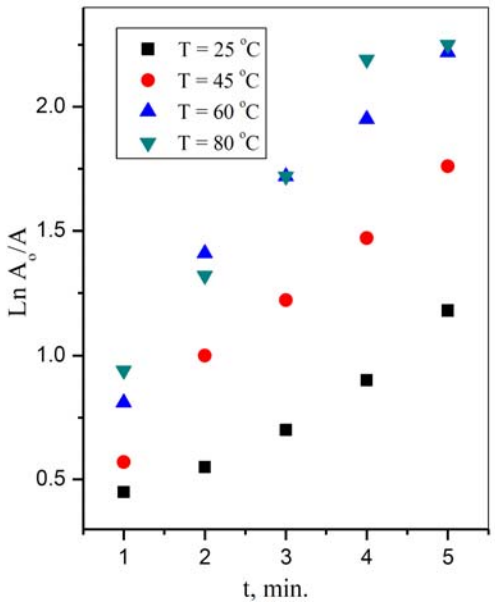
2.0
1.5
1.0
0.5
$\text{Ln } A_o/A$
1
2
3
4
5
t, min.
T = 25 °C
T = 45 °C
T = 60 °C
T = 80 °C

(d)

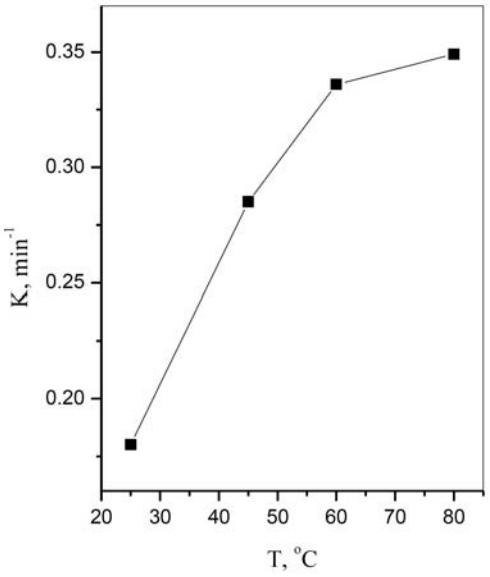

(e)

Figure 7. Effect of temperature on (a) removal percent (%R) of the dye, (b) pseudo first-order kinetic model, (c) pseudo second-order kinetic model (d) ln (A_o/A) for the catalytic degradation, and (e) change in reaction rate with temperature. (Catalyst concentration = 25mg/10ml, [MB] = 100ppm and pH = 7).

3.2.4. pH

Decolorizing reactions involving MnO_x catalyst were investigated within pH range 1.5-11 at 25ºC, [MB] 150mg/L and catalyst dose 25mg/10ml, as explained in Figure 8(a). The results obtained indicated that by decreasing pH from 11 to 1.5, the decolorization increases. This phenomenon can be explained as follow, the pH value of the aqueous solution not only affected on charge density of both adsorbent (MnO_x-G) and the adsorbate (MB) species, but also, the variation in the pH values will be influenced on the reduction potential of MnO_x according to Nernst equation (Equation (7)), which indicating that the decreasing in

the pH values leads to increase the reduction potential of MnO_x according to Equation (7):

$$MnO_2(s) + 4H^+ \leftrightarrow Mn^{2+}(aq) + 2H_2O,\ \varphi^\circ(MnO_2/Mn^{2+}) = 1.23V. \quad (7)$$

Moreover, the %R decreased with increasing pH, suggesting that the increase in density of surface complexes was not the predominant factor that control the oxidative decolorization of MB. Thus, pH causes a double edged effect on MB oxidation by controlling the surface complex formation and MnO_x reduction potential.

Furthermore, the larger %R results at lower pH than at higher pH refer to the effect of pH on the reduction potential rather than its effect on the surface complexation [5]. The kinetic data at different pH values obtained from the pseudo first order and pseudo second order kinetic models are found in Table 4. Values of R^2 and q_e calculated from pseudo first order model (Figure 8(b)) and pseudo second order kinetic model (Figure 8(c)) confirm that the experimental data fit very well pseudo second order kinetic model.

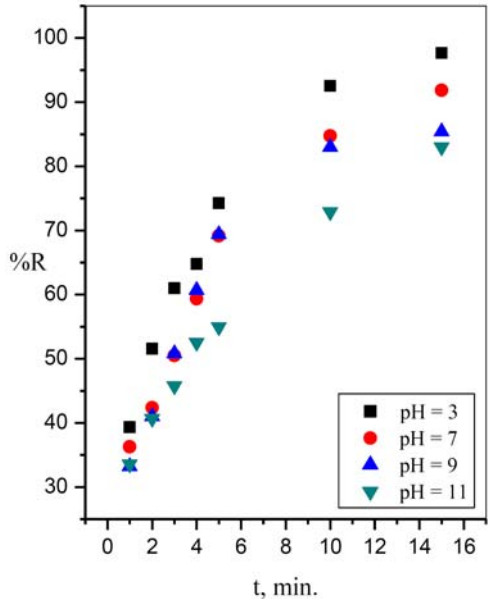

(a)

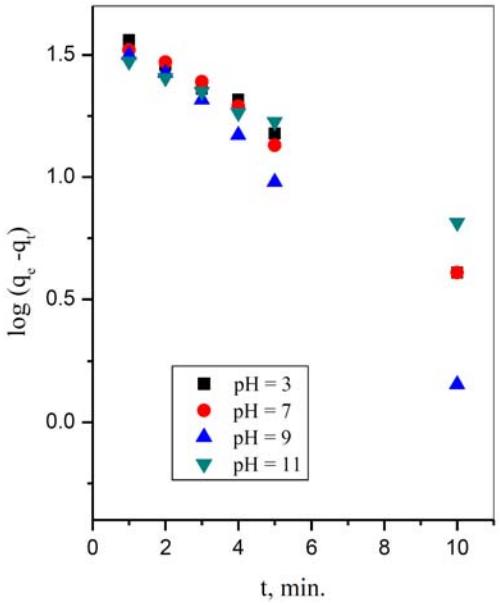

(b)

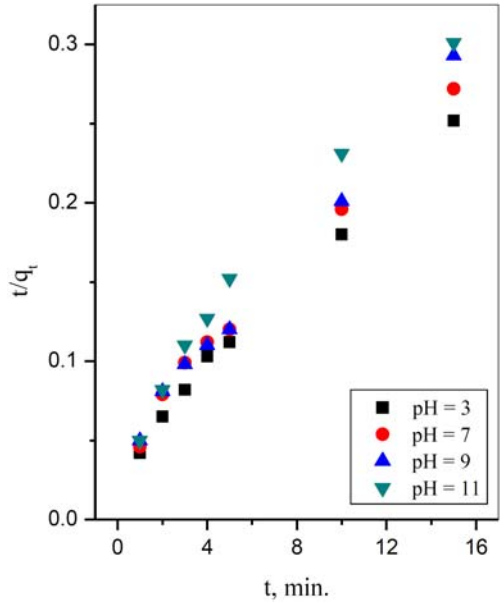
0.3
0.2
0.1
0.0
t/q_t
0
4
8
12
16
t, min.
pH = 3
pH = 7
pH = 9
pH = 11

(c)

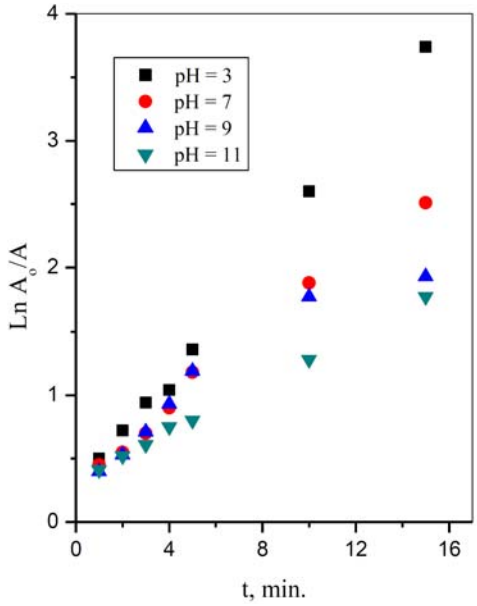
4
3
2
1
0
Ln A_o/A
0
4
8
12
16
t, min.
pH = 3
pH = 7
pH = 9
pH = 11

(d)

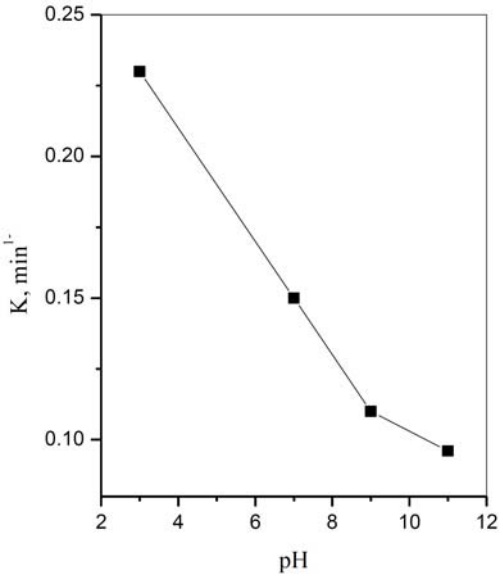

(e)

Figure 8. Effect of pH of solution on (a) removal percent (%R) of the dye, (b) pseudo first-order kinetic model, (c) pseudo second-order kinetic model (d) ln (A_o/A) for the catalytic degradation, and (e) change in reaction rate with pH value. (Catalyst concentration = 25mg/10ml, [MB] = 100ppm and T = 25°C).

Table 4. Calculated parameters of the pseudo first-order and pseudo second-order kinetic models for different pH values

pH	$q_{e\,\exp}$(mg/g)	First-order kinetic parameter		
		$K_1(\min^{-1})$	$q_{e\,\mathrm{cal}}$(mg/g)	R^2
3	59.59	– 0.25	49.00	0.990
7	55.12	– 0.24	46.77	0.990
9	51.26	– 0.35	55.00	0.990
11	49.83	– 0.17	36.31	0.993

pH	$q_{e\,\exp}$(mg/g)	Second-order kinetic parameter		
		$K_2(\mathrm{g\ mg^{-1}\ min^{-1}})$	$q_{e\,\mathrm{cal}}$(mg/g)	R^2
3	59.59	0.015	66.60	0.993
7	55.12	5.70×10^{-3}	62.50	0.990
9	51.26	0.017	58.22	0.994
11	49.83	0.020	50.00	0.972

By fitting the kinetic data obtained at different pH values in the pseudo first order rate Equation (6) gives Figure 8(d) and the slope of the linear graph gives the rate constants for each pH value. Figure 8(e) gives the relationship between the rate constants and different pH values, in which it is clear that decreasing the pH value is accompanied by decrease in the rate constant.

Several UV-Vis spectrum of MB-dye with time 0-15 min for the MB solution treated with MnO_x-G at pH 1.5 are displayed in Figure 9. From this figure, over time, the absorbance not only decreased but also $\lambda_{\max}$ was blue shifted from 664 (at zero time) to 552nm (after 15 min treating time). Wang et al. [20], had reported similar observation at using MnO_x-MB-dye system under microwave irradiation. Where, they indicated that maximum peak at 665nm was blue shifted to 618nm, 600nm, 588nm, and 562nm as a function of time.

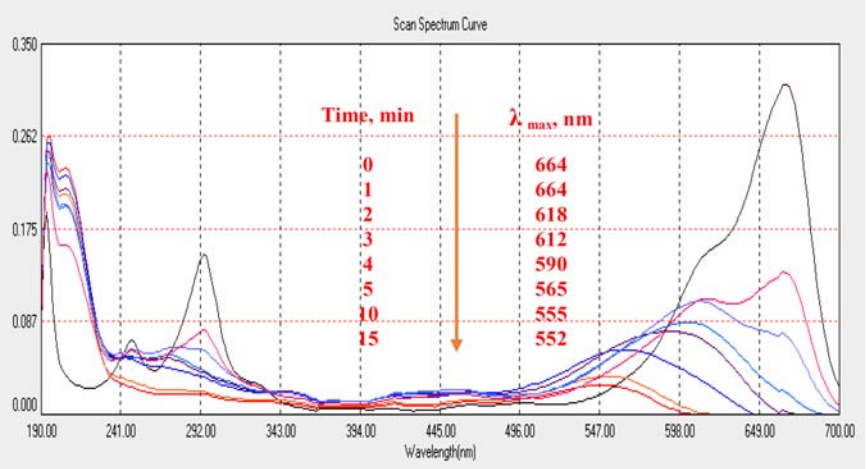

Figure 9. The UV-Vis spectra in the range of 190-700nm of MB-dye ([MB] = 100ppm, catalyst dose = 0.2g/20ml, T = 25ºC and pH = 1.5 for 0-15 min).

We can refer the shift in the maximum wave length (λ_{max}) to the presence of auxochromic alkylamine group in MB-dye, on one hand, the catalytic degradation of this type of the dye proceeded through N-dealkylation. On the other hand, the gradual degradation of all or part of auxochromic group (methyl or methyl amine) cause gradual decrease in color intensity and also blue shift [21, 22]. The change in the color of the dye as the treated time was prolonged (0-15 min.) with MnO_x-G at pH 1.5 was shown in Figure 10.

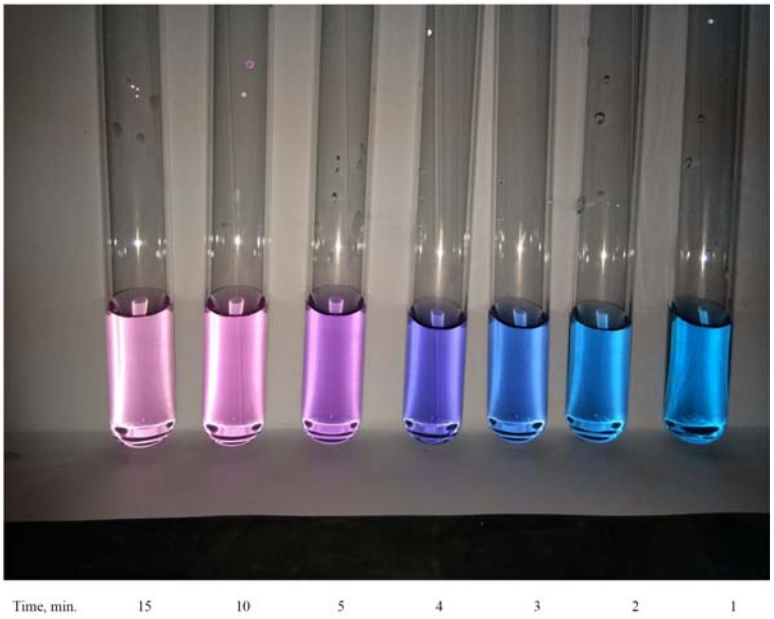

Figure 10. Change in the color of dye with the treated time of MnO_x-G ([MB] = 100ppm, catalyst dose = 0.2g/20ml, T = 25°C and pH = 1.5 for 0-15 min).

3.3. Comparison with different degradation systems

A comparison of the obtained MB degradation results in this paper on using MnO_x-G composite with other recent systems using copper, ruthenium, chromium, cobalt, and iron based oxides are reported in Table 5. From the data receded in the table, we can concluded that the composite prepared in this research consider to be more efficient and save the time more than the other used catalysis.

Table 5. Comparison of degradation of MB-dyes using various degradation systems

Catalyst	[MB]	[Dose]	time	[O.A]	%R	Ref.
CuO petals	0.2g/L	20mg/100ml	24 hr	200ml/L H_2O_2	95	[23]
CuO flowers	0.2g/L	20mg/100ml	24 hr	200ml/L H_2O_2	72	[23]
$[Ru^{III}(hedtra)(H_2O)]$	0.05mM	0.05mM	10 min	20mM H_2O_2	99.9	[24]
CrO(OH) NPs	200mg/L	0.04g/10ml	30 min	--	80	[25]
CrO(OH) NPs	200mg/L	0.04g/10ml	10 min	100ml/L H_2O_2	80	[25]
CuO	10mg/L	10mg	60 min	200ml NaOCl	100	[26]
Co-oxide	50mg/L	0.5g/L	25 min	45g/L NaOCL	100	[27]
Fe Co-oxide	50mg/L	0.5g/L	40 min	45g/L NaOCL	100	[27]
Fe Co-oxide	50mg/L	0.5g/L	60 min	45g/L NaOCL	72	[27]
MnO_x-G	100mg/L	25mg/10ml	10 min	--	99.5	This work

4. Conclusions

This paper states an easy preparation of a highly active MnO_x-G catalytic composite. The composite was prepared by one-step wet milling approach and used as a catalyst in the catalytic degradation of the MB dye. Based on the calculated and experimental q_e and R^2 values obtained from different experimental conditions, the pseudo second-order kinetic model was suggested to describe the kinetic of adsorption step. The catalytic degradation of MB dye was fitted by pseudo first-order kinetic model according to L-H model. The rate of catalytic degradation was increased with the increase in composite dose to a certain point (25mg) after which the rate decreased. Also, the degradation rate increases with rising in the temperature, while the degradation rate decreases with further increasing in the dye concentration and pH value.

References

[1] L. Zhu, Z. Meng, C. Park, T. Ghosh and W. Oh, Characterization and relative sonocatalytic efficiencies of a new MWCNT and CdS modified TiO_2 catalysts and their application in the sonocatalytic degradation of rhodamine B, Ultrasonics Sonochemistry 20(1) (2013), 478-484.

DOI: https://doi.org/10.1016/j.ultsonch.2012.08.005

[2] J. Yu, B. Li, X. Sun, Y. Jun and R. Chi, Adsorption of methylene blue and rhodamine B on baker's yeast and photocatalytic regeneration of the biosorbent, Biochemical Engineering Journal 45(2) (2009), 145-151.

DOI: https://doi.org/10.1016/j.bej.2009.03.007

[3] W.-H. Kuan and Yen-Chuan Chan, pH-dependent mechanisms of methylene blue reacting with tunneled manganese oxide pyrolusite, Journal of Hazardous Materials 239(240) (2012), 152-159.

DOI: https://doi.org/10.1016/j.jhazmat.2012.08.051

[4] M. Rafatullah, O. Sulaiman, R. Hashim and A. Ahmad, Adsorption of methylene blue on low-cost adsorbents: A review, Journal of Hazardous Materials 177(1-3) (2010), 70-80.

DOI: https://doi.org/10.1016/j.jhazmat.2009.12.047

[5] M.-X. Zhu, Z. Wang, S.-H. Xu and T. Li, Decolorization of methylene blue by δ-MnO_2-coated montmorillonite complexes: Emphasizing redox reactivity of Mn-oxide coatings, Journal of Hazardous Materials 181(1-3) (2010), 57-64.

DOI: https://doi.org/10.1016/j.jhazmat.2010.04.080

[6] B. J. Lafferty, M. Ginder-Vogel and D. L. Sparks, Arsenite oxidation by a poorly-crystalline manganese oxide 3: Arsenic and manganese desorption, Environmental Science & Technology 45(21) (2011), 9218-9223.

DOI: https://doi.org/10.1021/es201281u

[7] D. B. Loomer, T. A. Al, V. J. Banks, B. L. Parker and K. U. Mayer, Manganese valence in oxides formed from in situ chemical oxidation of TCE by $KMnO_4$, Environmental Science & Technology 44(15) (2010), 5934-5939.

DOI: https://doi.org/10.1021/es100879w

[8] Z. Yang, Y. Zhang, W. Zhang, X. Wang, Y. Qian, X. Wen and S. Yang, Nanorods of manganese oxides: Synthesis, characterization and catalytic application, Journal of Solid State Chemistry 179(3) (2006), 679-684.

DOI: https://doi.org/10.1016/j.jssc.2005.11.028

[9] W. Zhang, Z. Yang, X. Wang, Y. Zhang, X. Wen and S. Yang, Large-scale synthesis of β-MnO_2 nanorods and their rapid and efficient catalytic oxidation of methylene blue dye, Catalysis Communications 7(6) (2006), 408-412.

DOI: https://doi.org/10.1016/j.catcom.2005.12.008

[10] Stanton Ching, Katarzyna S. Krukowska and Steven L. Suib, A new synthetic route to todorokite-type manganese oxides, Inorganica Chimica Acta 294(2) (1999), 123-132.

DOI: https://doi.org/10.1016/S0020-1693(99)00208-X

[11] S. Lagergren, K. Sven. Vetenskapsakad. Handlingar Band 24 (1898), 1-39.

[12] Y. S. Ho and G. McKay, The sorption of lead(II) ions on peat, Water Research 33(2) (1999), 578-584.

DOI: https://doi.org/10.1016/S0043-1354(98)00207-3

[13] H. Chen, P. K. Chu, J. He, T. Hu and M. Yang, Porous magnetic manganese oxide nanostructures: Synthesis and their application in water treatment, Journal of Colloid and Interface Science 359(1) (2011), 68-74.

DOI: https://doi.org/10.1016/j.jcis.2011.03.089

[14] L. Youji, Z. Xiaoming, C. Wei, L. Leiyong, Z. Mengxiong, Q. Shidong and S. Shuguo, Photodecolorization of rhodamine B on tungsten-doped TiO_2/activated carbon under visible-light irradiation, Journal of Hazardous Materials 227-228 (2012), 25-33.

DOI: https://doi.org/10.1016/j.jhazmat.2012.04.071

[15] C. F. Cano-Guzmán, J. P. Pérez-Orozco, I. Hernández-Pérez, L. González-Reyes, V. Garibay-Febles and R. Suárez-Parra, Kinetic study for reactive red 84 photo degradation using iron (III) oxide nanoparticles in annular reactor, Journal of Textile Science & Engineering 4(2) (2014), 1-8.

DOI: https://doi.org/10.4172/2165-8064.1000155

[16] M. A. Lazar, S. Varghese and S. S. Nair, Photocatalytic water treatment by titanium dioxide: Recent updates, Catalysts 2(4) (2012), 572-601.

DOI: https://doi.org/10.3390/catal2040572

[17] V. S. Suvith and D. Philip, Catalytic degradation of methylene blue using biosynthesized gold and silver nanoparticles, Spectrochimica Acta Part A: Molecular and Biomolecular Spectroscopy 118 (2014), 526-532.

DOI: https://doi.org/10.1016/j.saa.2013.09.016

[18] M. Das and K. G. Bhattacharyya, Oxidation of rhodamine B in aqueous medium in ambient conditions with raw and acid-activated MnO_2, NiO, ZnO as catalysts, Journal of Molecular Catalysis A: Chemical 391 (2014), 121-129.

DOI: https://doi.org/10.1016/j.molcata.2014.04.019

[19] B. N. Patil, D. B. Naik, V. S. Shrivastava, Photocatalytic degradation of hazardous Ponceau-S dye from industrial wastewater using nanosized niobium pentoxide with carbon, Desalination 269(1-3) (2011), 276-283.

DOI: https://doi.org/10.1016/j.desal.2010.11.014

[20] X. Wang, L. Mei, X. Xing, L. Liao, G. Lv, Z. Li and L. Wu, Mechanism and process of methylene blue degradation by manganese oxides under microwave irradiation, Applied Catalysis B: Environmental 160-161 (2014), 211-216.

DOI: https://doi.org/10.1016/j.apcatb.2014.05.009

[21] T. Y. Zhang, T. Oyama, S. Horikoshi, H. Hidaka, J. C. Zhao and N. Serpone, Photocatalyzed N-demethylation and degradation of methylene blue in titania dispersions exposed to concentrated sunlight, Solar Energy Materials and Solar Cells 73(2) (2002), 287-303.

DOI: https://doi.org/10.1016/S0927-0248(01)00215-X

[22] G. Cheng, L. Yu, T. Lin, R. Yang, M. Sun, B. Lan, L. Yang and F. Deng, A facile one-pot hydrothermal synthesis of β-MnO_2 nanopincers and their catalytic degradation of methylene blue, Journal of Solid State Chemistry 217 (2014), 57-63.

DOI: https://doi.org/10.1016/j.jssc.2014.04.025

[23] S. Zaman, A. Zainelabdin, G. Amin, O. Nur and M. Willander, Efficient catalytic effect of CuO nanostructures on the degradation of organic dyes, Journal of Physics and Chemistry of Solids 73(11) (2012), 1320-1325.

DOI: https://doi.org/10.1016/j.jpcs.2012.07.005

[24] D. Chatterjee and A. Katafias, Degradation of methylene blue by $[Ru^{III}(hedtra)(H_2O)]/H_2O_2$ catalytic system, Current Catalysis 3(1) (2014), 82-87.

DOI: https://doi.org/10.2174/15748936113086660019

[25] R. Azmat and A. Saeed, Catalytic degredation of methylene blue by nanostructured CrO(OH) prepared by hydrothermal method, European Chemical Bulletin 3(5) (2014), 417-421.

DOI: http://dx.doi.org/10.17628/ecb.2014.3.417-421

[26] A. El Farrouji, A. C. Eddine, S. E. Bouzit, B. Boualy, A. Mehdi, L. El Firdoussi and M. A. Ali, Degradation of methylene blue using synthesized nanostructured CuO with high specific surface area through catalytic oxidation, International Research Journal of Pure & Applied Chemistry 8(4) (2015), 190-197.

DOI: https://doi.org/10.9734/IRJPAC/2015/18057

[27] M. Stoyanova and S. Christoskova, Catalytic degradation of methylene blue in aqueous solutions over Ni– and Co– oxide systems, Central European Journal of Chemistry 9(6) (2011), 1000-1007.

DOI https://doi.org/10.2478/s11532-011-0086-7

■